SQUWA: Signal Quality Aware DNN Architecture for Enhanced Accuracy in Atrial Fibrillation Detection from Noisy PPG Signals

Runze Yan RUNZE.YAN@EMORY.EDU
Center for Data Science, Nell Hodgson Woodruff School of Nursing, Emory University
Ding Cheng CHENGDING@GATECH.EDU
Department of Biomedical Engineering, Georgia Institution of Technology & Emory University
Ran Xiao RAN.XIAO@EMORY.EDU
Center for Data Science, Nell Hodgson Woodruff School of Nursing, Emory University
Aleksandr Fedorov ALEKSANDR.VLADIMIROVICH.FEDOROV@EMORY.EDU
Center for Data Science, Nell Hodgson Woodruff School of Nursing, Emory University
Randall J Lee RANDALL.LEE@UCSF.EDU
School of Medicine, University of California at San Francisco
Fadi B Nahab FNAHAB@EMORY.EDU
Department of Neurology, School of Medicine, Emory University
Xiao Hu XIAO.HU@EMORY.EDU
Center for Data Science, Nell Hodgson Woodruff School of Nursing, Emory University

Abstract

Atrial fibrillation (AF), a common cardiac arrhythmia, significantly increases the risk of stroke, heart disease, and mortality. Photoplethysmography (PPG) offers a promising solution for continuous AF monitoring, due to its cost efficiency and integration into wearable devices. Nonetheless, PPG signals are susceptible to corruption from motion artifacts and other factors often encountered in ambulatory settings. Conventional approaches typically discard corrupted segments or attempt to reconstruct original signals, allowing for the use of standard machine learning techniques. However, this reduces dataset size and introduces biases, compromising prediction accuracy and the effectiveness of continuous monitoring. We propose a novel deep learning model, **S**ignal **Qu**ality **W**eighted Fusion of **A**ttentional Convolution and Recurrent Neural Network (SQUWA), designed to learn how to retain accurate predictions from partially corrupted PPG. Specifically, SQUWA innovatively integrates an attention mechanism that directly considers signal quality during the learning process, dynamically adjusting the weights of time series segments based on their quality. This approach enhances the influence of higher-quality segments while reducing that of lower-quality ones, effectively utilizing partially corrupted segments. This approach represents a departure from the conventional methods that exclude such segments, enabling the utilization of a broader range of data, which has great implications for less disruption when monitoring of AF risks and more accurate estimation of AF burdens. Moreover, SQUWA utilizes variable-sized convolutional kernels to capture complex PPG signal patterns across different resolutions for enhanced learning. Our extensive experiments show that SQUWA outperform existing PPG-based models, achieving the highest AUCPR of 0.89 with label noise mitigation. This also exceeds the 0.86 AUCPR of models trained with using both electrocardiogram (ECG) and PPG data.

Data and Code Availability Research data will not be shared for ethical reasons, except for one publicly accessible. The detailed data description are in Section 4.1. Code is available at https://github.com/Runz96/SQUWA.

1. Introduction

Atrial Fibrillation (AF), the most common chronic cardiac arrhythmia, impacts around 33.5 million people globally, with its occurrence increasing Chugh et al. (2014). Notably, AF significantly contributes

to health risks, accounting for 20% of all strokes and a third of all hospital admissions due to heart rhythm issues Marini et al. (2005). Early detection of AF is crucial to lower its associated risks, allowing for timely intervention that can slow the progression of electrical and structural changes in atrial tissue Hart et al. (2007). While electrocardiogram (ECG) signals are the gold standard for detecting AF, their use is constrained by issues with long-term daily wearability. This limitation drives the search for alternative signal types, like photoplethysmography (PPG), to monitor and detect AF Charlton et al. (2023). PPG signals represent blood volume changes in the microvascular bed of tissue, providing a non-invasive method to capture the characteristics of irregular heart rhythms of AF. Their potential for AF detection, combined with their presence in about 71% of consumer wearables has highlighted their significance Henriksen et al. (2018). However, the utility of PPG in AF detection is often undermined by noise such as motion artifacts Seok et al. (2021). Thus, accurate classification of these noise-affected PPG signals is critical for the development of a system that is both highly sensitive and precise in detecting AF, in particular for screening AF at scale.

Despite progress in AF detection using PPG data with Deep Neural Networks (DNNs) like Convolutional Neural Networks (CNN) Shashikumar et al. (2017), Long Short-Term Memory (LSTM) Cheng et al. (2020), and Transformer Neural Networks Nankani and Baruah (2022), the challenge of noise and motion artifacts in raw PPG signals persists. Current methods for the corrupted PPG signals involves discarding low-quality samples, or enhancing the signal-to-noise ratio (SNR), so that the standard neural network methods can focus on the 'clean' data and tend to ignore signals that are not of high quality Liaqat et al. (2020). However, discarding low-quality signals can reduce the volume of data available for model training, leading to challenges in estimating metrics like AF burden Pereira et al. (2019b); Zhu et al. (2021). This strategy often relies on arbitrary thresholds to remove low-quality signals Roy et al. (2020). Other approaches attempt to improve signal quality before detecting AF, which can lead to errors accumulation and propagation from the enhancement stage to detection, potentially compromising the algorithm's effectiveness Ding et al. (2023); Yan et al. (2022); Afandizadeh Zargari et al. (2023). On the other hand, a one-step method that incorporates PPG signal quality directly into the AF detection process could be more efficient. This approach enhances accuracy by fully utilizing the training data without modifying the raw signal.

In this study, we introduce a novel DNN architecture, termed **S**ignal **Qu**ality **W**eighted Fusion of **A**ttentional Convolution and Recurrent Neural Network (SQUWA), designed for AF detection using PPG data. Unlike conventional methods that exclude low-quality signals, SQUWA integrates an innovative attention mechanism that dynamically assigns weights to PPG segments based on their signal qualities. This mechanism is not an isolated feature but is integrated into the AF detection process. It is designed to account for signal quality levels within the learning model, avoiding the separate, two-step approaches. In practice, during AF detection, SQUWA gives more weight to high-quality segments and reduces the influence of noisy segments. This approach allows SQUWA make the most of high-quality segments in a PPG sample, reducing the effect of lower-quality parts on the overall analysis and ensuring the model's predictions are based on the most reliable data. Furthermore, this attention mechanism works at a detailed temporal resolution, processing each data point independently rather than treating an entire PPG sample as a homogeneous unit. This refined approach enhances the overall effectiveness and accuracy of the AF detection process.

Additionally, to support this attention mechanism, we utilize a class activation map (CAM) Zhou et al. (2016) derived from a pre-trained signal quality (SQ) model. This CAM generates a continuous signal quality index (SQI) for each PPG signal, offering a granular view of signal quality over time Pereira et al. (2019a). Another novel feature of SQUWA is the initial decomposition of a PPG signal. This involves decomposing the raw signal and its first and second derivatives using a variety of CNN kernels, each with different kernel sizes. These decomposed elements are then strategically reassembled by a sub-network to create a composite signal. This approach is crucial in highlighting relevant signal features, significantly improving the ability to distinguish between AF and non-AF conditions.

Our training and testing approach is meticulously designed to enhance the model's robustness and generalizability. We train the model on over 5 million PPG samples, ensuring comprehensive learning that covers a variety of etiological variations in the disease population. For testing, we rigorously assess it on three separate external datasets, validat-

ing its adaptability and effectiveness across different real-world scenarios. Experimental results show that our approach improves AF detection accuracy, even with fluctuating signal quality. The SQUWA method outperforms baseline models, including CNN and RNN-based single-modality AF detection neural networks, across three external test sets. Remarkably, our method also shows competitive results when compared to an AF detection model trained using both PPG and ECG data. To our best knowledge, the proposed approach is the first deep learning framework that considers signal quality as an integral element in learning an AF detector. The contribution of this work can be summarized as follows:

- We implemented an attention mechanism that accounts for both PPG signal quality and AF detection. This approach prioritizes segments with higher SQIs, enabling accurate AF classification even when PPG signals are partly compromised.
- The SQUWA model uses an adaptive attention sub-network that integrates the raw PPG signal with its first and second derivatives. This setup lets the model examine the signal's rate of change and curvature, offering a complete view of the signal's dynamics.
- The proposed method outperforms the baseline PPG models, and our model interpretation analysis shows that SQUWA assigns higher attention weights to high-quality PPG segments.

2. Related Work

Recent progress in model design has focused on addressing the challenges posed by noisy signals. This includes strategies for both preprocessing—to improve signals before classification—and post-processing, aimed at refining predictions to offset the impact of partially corrupted data segments. Chatterjee et al. (2020); Zhang et al. (2021a). The following paragraphs will highlight the strengths and weaknesses of common techniques within these two categories.

A notable preprocessing strategy for signal denoising involves the use of Variational Autoencoders (VAEs) and Generative Adversarial Networks (GANs) to augment data Im Im et al. (2017); Brophy et al. (2023). These models have shown promise in restoring corrupted data of various types, such as images Im Im et al. (2017), acoustic signals Kuo et al. (2020), and text Zhu et al. (2018). Denoising GAN (DN-GAN) Chen et al. (2020) and Denoising Autoencoders Bengio et al. (2013) have been explored for their capacity to learn complex, high-level representations of data and for their ability to filter out noise, respectively. However, their success relies on the assumption that the noise patterns are predictable or follow certain distributions. This assumption may not hold in real-world scenarios where noise and corruption can be unpredictable and non-uniform.

Transfer Learning has also been utilized to mitigate the challenges of partially corrupted signals Pan and Yang (2009). Zhang et al. (2020) leveraged a pretrained models on a clean speech dataset and adapted them to specific speech recognition task with lower quality data. Kim et al. (2020) has utilized transfer learning to address the challenges by training a network with synthetic noise and then transferring this knowledge to effectively handle the varying characteristics of real-world noise. However, the effectiveness of transfer learning is limited by the availability of representative training data and the discrepancies between training and application datasets Day and Khoshgoftaar (2017). Models trained on high-quality data often struggle to adapt to lower quality signals, leading to challenges in accurately interpreting biomedical signals like PPG-based AF detection Pan and Yang (2009). Significant discrepancies in data quality and patient demographics often require time-consuming fine-tuning and domain adaptation.

Attention mechanisms are designed to direct a model's focus to the most significant parts of the input, improving learning efficiency and accuracy. Niu et al. (2021). Attention methods have been successfully applied in many tasks, e.g., machine translation Tan et al. (2020), computer vision Guo et al. (2022), and even physiological signals for AF detection Mousavi et al. (2020). A closely related study introduced a unique heart rate estimation method that combines a signal quality attention mechanism with an LSTM network Gao et al. (2022), which proposed a novel remote heart estimation algorithm from video. However, this approach only uses attention mechanisms for offline correction of heart rate data, not for integrating signal quality into the learning phase. While attention mechanisms can aid in leveraging high-quality segments and reducing biases from low-quality ones, their use in addressing the challenges of making predictions from partially corrupted data remains unexplored.

3. Methods

Figure 1 visualizes the overall structure of SQUWA, which begins by generating a composite signal from the raw PPG and its first and second derivatives. This process involves the use of variable-sized kernels to break down these signals. Subsequently, an attention subnet aggregates the kernel outputs through a weighted sum. A deep CNN then processes this composite signal to extract features with a lower temporal dimension to facilitate the subsequent temporal integration through a LSTM. Moreover, a pre-trained CNN-based signal quality (SQ) model evaluates the raw PPG signal, producing a signal quality index (SQI) over time. These LSTM outputs and SQIs are then combined through a signal quality attention (SQ-attention) mechanism. This nuanced integration of both signal features and SQIs weighs more contributions from locations in the signal where SQIs are high so that valuable information from partially corrupted PPG signals is effectively utilized for accurate classification. End-to-end training of SQUWA enables this data-driven integration process to maximize sensitivity and minimize false detection.

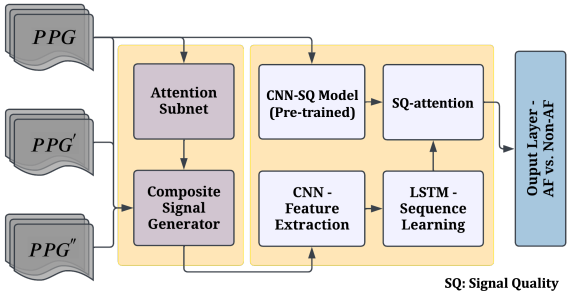

Figure 1: Structure of Signal Quality Weighted Fusion of Attentional Convolution and Recurrent Neural Network (SQUWA).

3.1. Composite Signal Generation

The composite signal generation incorporates the two components found within the yellow box on the left side of Figure 1. The inputs of the SQUWA network are the raw PPG signal and its first and second derivatives. A PPG signal captures the heart's pulse by tracking changes in blood volume with each beat. The first derivative of the PPG signal relates to the velocity of the blood flow, indicating the rapidity of blood volume changes within the vessels and mirroring the pulse's rhythm. The second derivative offers a deeper look at how quickly the blood flow's velocity changes, essentially gauging the acceleration or deceleration of blood within the vessels. As shown in Figure 3.1, these three forms of the PPG signal are analyzed in parallel by convolutional kernels of three different lengths ranging from a short to a long scale. The exact length of the kernel and the number of kernels will be fine-tuned during the training process, but the goal is to decompose the input at different scales and learn how to selectively combine them into a composite signal. The output from all kernels of the same length will be combined by using a 1x1 kernel, and this process results in nine component signals of the same length as that of the original PPG. An attention subnet learns weights to combine these nine components in a way that is determined by the characteristics of raw PPG. This attention subnet includes a convolutional layer, a fully-connected layer, and a SoftMax layer.

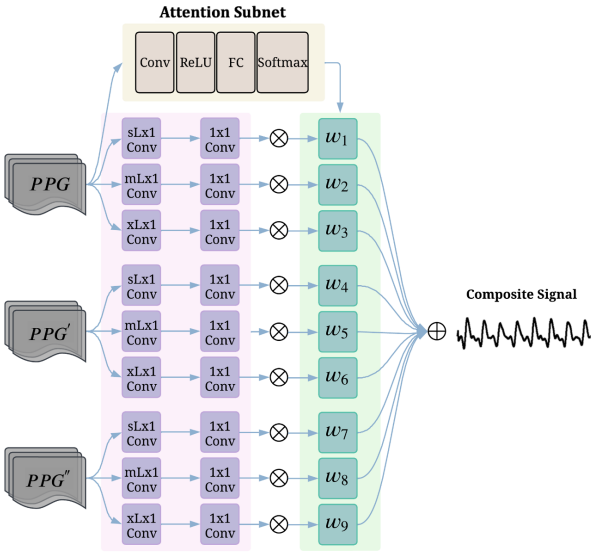

Visualization of the composite signal generation in the proposed SQUWA algorithm.

3.2. CNN-LSTM Fusion

Figure 2 highlights two branches: one for processing the composite signal and the other for processing the raw PPG. The composite signal is analyzed by a CNN to effectively extract a sequence of feature

vectors. These vectors have a dimension of $n \times T$, where n is the number of kernels in the last convolutional layer and T is the temporal dimension of the sequence. Because of pooling layers in the CNN, T will be smaller than the length of the original signal. The second branch uses a CNN-based SQ model that processes raw PPG signals to produce SQIs. This SQ model, pre-trained on a small PPG dataset labeled with good and bad signal quality, differentiates between these qualities. We utilized the class activation map (CAM) from the last layer (prior to a global average pooling layer) of the SQ model as SQIs to reflect PPG quality over time Zhang et al. (2021b). To match the temporal dimension with the feature-extraction CNN, we make sure the downsampling factors in both CNN networks are identical so that each element of a feature sequence from the first branch can be characterized by a scalar SQI. We use 1-D ResNet as the backbone for the CNN feature extraction layer and SQ model and leave the exploration of other more modern CNN architecture for future work Alzubaidi et al. (2021). These two networks do not need to have identical architectures but need to have the same downsampling factors to be temporally in sync. The output of the CNN feature extractor will be processed by a LSTM, and we use the one-directional LSTM as the backbone. The output from the LSTM has the dimension of $k \times T$, where k is the number of hidden units in the LSTM layer.

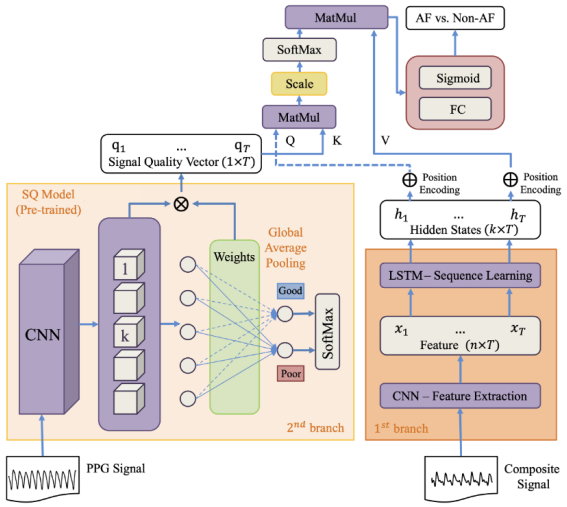

Figure 2: Visualization of the CNN-LSTM fusion and SQ-attention process.

3.3. Signal Quality (SQ) - Attention

In this section, we introduced the SQ-attention mechanism that begins by analyzing the hidden states H from the LSTM, which captures the temporal sequential patterns in the PPG signal, along with signal quality values SQI that assess the quality of each segment of the PPG signal in Figure 2. As shown in Formula 1, the mechanism converts these hidden states H and SQI values into queries (Q), keys (K), and values (V), which are simplified representations to help the model determine the segments of the signal that should be prioritized.

$$\begin{aligned} H_{\text{adj}} &= H + P \\ Q &= H_{\text{adj}}^T \cdot W_Q \\ K &= SQI^T \cdot W_K \\ V &= H_{\text{adj}}^T \cdot W_V \end{aligned} \tag{1}$$

, where W_Q, W_K, and W_V are the weight matrices for the query, key, and value transformation, respectively. And P represents the positional encoding.

The attention mechanism operates by pairing queries with keys. This is done by measuring how much each query matches with a key, taking the product of two numbers in Formula 2. This step calculates the significance or 'weight' to be assigned to each segment of the signal, which we call attention scores S_{atten}. The weight matrices W_Q and W_V are shaped $(k \times k)$, and weight matrix W_K is sized $(1 \times k)$. Given that the hidden states from LSTM has the dimension $(k \times T)$ and signal quality vector has the dimension $(1 \times T)$, the dimension of S_{atten} is $(T \times T)$.

$$S_{atten} = \frac{QK^T}{\sqrt{d_k}} \tag{2}$$

, where d_k normalizes the attention scores, equal to k, the number of hidden units in the LSTM layer.

$$W_{atten} = \text{SoftMax}(S_{atten}) \tag{3}$$

Formula 3 uses a softmax function to convert the attention scores into a standardized form where they all sum to one, thus scaling attention across the signal. The resulting scores form the attention matrix W_{atten}, which, as shown in Formula 4, is used to calculate a context vector by weighting the value vectors according to these scores.

$$\text{Output} = W_{atten} \cdot V \tag{4}$$

This output context vector is a refined summary of

the entire PPG signal, adjusted according to the quality of the signal. It emphasizes the trustworthy segments of the signal while diminishing the influence of lower quality parts. Finally, the context vector goes through a fully connected layer and a sigmoid function, which together classify the PPG signal. The sigmoid function provides the probability of the signal belonging to a specific category, thus completing the process of integrating SQIs into PPG signal classification.

4. Experiment

4.1. Dataset

In this study, we employed a comprehensive evaluation on multiple datasets. For training purposes, we used a large-scale dataset, and for evaluation, we utilized three additional external datasets, including one that is publicly available. Additionally, we incorporated a smaller signal quality dataset with clean labels and detailed signal quality information, such as the presence and exact timings of low-quality segments. This dataset was used to train our signal quality assessment model.

4.1.1. Train dataset

Our training dataset was sourced from 28,539 patients in a hospital environment, where continuous PPG signals were recorded from bedside monitors. These monitors flagged events such as atrial fibrillation (AF), premature ventricular contraction (PVC), and others. Our study focused on AF, PVC, and normal sinus rhythm (NSR), grouping PVC and NSR labels under Non-AF for a binary AF vs. Non-AF classification. The PPG signals were segmented into non-overlapping 30-second intervals, initially sampled at 240Hz (7,200 timesteps each), and then downsampled to 80Hz (2,400 time steps). The dataset was divided by patient IDs into training and validation sets. The training dataset included 13,432 patients with 2,757,888 AF and 3,014,334 Non-AF segments, while the validation set comprised 6,616 patients with 1,280,775 AF and 1,505,119 Non-AF segments. Given that the labels were automatically generated by monitors, some label noise is expected and estimated to be around 25%. This estimate was derived by manually annotating a small sample of the dataset Ding et al. (2024).

4.1.2. Signal quality dataset

The signal quality dataset consists of 18,055 PPG segments from 13 stroke patients Pereira et al. (2019a). The data collection settings for this dataset were consistent with those of our training dataset. A notable feature of this dataset is the detailed information on signal quality, including the presence and specific timings of segments with poor quality. The SQ model shown in Figure 1 was trained using this dataset.

4.1.3. Test dataset

Testset A (Public Source) Testset A is a public dataset from Torres-Soto and Ashley (2020), featuring data from wrist-worn devices in ambulatory settings. Originally with 25-second segments, we augmented these to 30 seconds and resampled them to 2,400 timesteps. It contains 52,911 AF and 80,620 Non-AF samples from 163 patients, including those with AF and healthy individuals.

Testset B (Institution B) Sourced from institution B, Testset B was gathered using wrist-worn Samsung Simband devices from 98 ambulatory patients. We processed the data into 30-second segments with 2,400 timesteps each. The dataset includes 348 AF and 506 Non-AF segments, reviewed and annotated by medical professionals.

Testset C (Institution C) Testset C, collected from institution C, consists of fingertip PPG data from 126 hospital patients. We formatted the continuous signals into 30-second, non-overlapping segments, each downsampled to 2,400 timesteps. This dataset includes 38,910 AF and 220,740 Non-AF segments, annotated by cardiac electrophysiologists.

4.2. Compared Model

To evaluate the performance of our proposed model, we conduct a performance comparison against several baseline models, including ResNet-34 classifer He et al. (2016), LSTM model Yu et al. (2019) and the hybird ResNet-34 and LSTM architecture. Moreover, we also include two recent AF detection models that are publicly accessible: the CMC model, which addresses the issues of inaccurate AF labels Ding et al. (2024), and anther model SiamAF, which is trained utilizing both PPG and ECG data but only utilizing PPG for inference Guo et al. (2023). Given the presence of noisy label in our training dataset, as discussed in Section 4.1, we apply a variety of label noise

mitigation techniques, including the strategy used in CMC study Ding et al. (2024), Symmetric Cross Entropy (SCE) Wang et al. (2019), Joint Optimization Learning (JOL) Tanaka et al. (2018), and Generalized Cross Entropy (GCE) Zhang and Sabuncu (2018). We utilized Area Under the Receiver Operating Characteristic curve (AUROC), F1 score, and Area Under the Precision-Recall Curve (AUCPR) as metrics to compare the performance of SQUWA with several baselines.

4.3. Ablation Study

To rigorously evaluate our SQUWA model, we performed a series of ablation studies, as outlined in Table 1. These experiments involved systematically removing certain components of the model to create different model variants to assess their individual contributions. We also removed different sized kernels from the signal compositor to see the effect of each. The NKS, NKM, and NKL variants were each modified by removing (N) the small (S), medium (M), and large (L) kernels (K), respectively. The NSC variant was designed to use the raw PPG signal directly, bypassing the composite signal (SC) as input. In the NFE variant, we took away the CNN that extracts features (FE) and let the composite signal be analyzed by the LSTM. For the NRN variant, we replaced the LSTM with a simpler global averaging layer with SQI integration. The NSQ variant retained the CNN and LSTM combination but did not incorporate SQIs, to specifically assess the role of signal quality integration. Finally, to further explore the significance of SQI integration, we introduced the RSQ variant. This model has the complete SQUWA structure but is trained with randomly (R) generated SQIs, enabling us to evaluate the impact of accuracy of SQIs on model performance.

5. Results

The results in Table 2 show that SQUWA outperforms ResNet, LSTM, and the combined ResNet-34 + LSTM in terms of all three metrics across different test sets. CMC, a recent model tailored for AF detection using PPG signals known for its ability to manage label noise, is outperformed by our SQUWA model, despite SQUWA not being specifically designed to handle label noise. This is an important observation given that our training dataset is affected by label noise. Comparing SQUWA with SiamAF, a contemporary AF detection model trained using both PPG and ECG data, SQUWA shows competitive performance on Testsets B and C. However, it does not perform as well on Testset A. Furthermore, the last four rows of the table show SQUWA's performance when combined with strategies to address the label noise, such as the strategy used in the CMC model, as well as other methods like SCE, JOL, and GCE. Notably, these strategies improve SQUWA's performance, allowing it to surpass SiamAF on Testset A. For instance, SQUWA with JOL achieves a F1 score of 0.63 on Testset A, which is higher than the 0.61 F1 score from SiamAF.

In the ablation study, we evaluate the performance of SQUWA against a series of its modified versions. As shown in Figure 3, the AUCPR metric is utilized to compare these models across three distinct datasets. From the results, it is apparent that the full SQUWA model generally outperforms its ablated counterparts. This suggests that all parts of the model work well together to make accurate predictions. For example, the version without the CNN for handling composite signals, named NFE, shows a notable decrease in performance across all datasets. This tells us that using a CNN to get features from PPG signals is important. When we look at how the model does with different kernel sizes in the signal compositor, we observe varying degrees of performance drop. The version with a medium-sized kernel, NKM, didn't do as poorly as the versions with small or large kernels. This means the medium-sized kernel might not be as important as the other two kernel sizes. However, the large kernel seems more important for the Testset B and Testset C, but not as much for Testset A, where it's about as important as the small kernel. Another interesting point is that the version NSQ without the signal quality integration, which is key for managing noisy data, had a significant drop in performance, especially in Testset A. The RSQ version, characterized by its randomly generated signal quality index, exhibited the poorest performance among all variants across the three datasets. These findings underscore the crucial role of signal quality. On the other hand, the NRN version didn't fall behind much from the full SQUWA model. Overall, these observations suggest that each component of the SQUWA model plays a vital role in its overall effectiveness, with certain components being particularly critical depending on the datasets evaluated.

Table 1: Configuration for the ablation study, where 'x' denotes the inclusion of specific modules in the algorithm, and 'N/A' indicates the absence of such modules. SC means composite signal generation.

	sLx1 Conv	mLx1 Conv	xLx1 Conv	SC	CNN	LSTM	SQ-attention
SQUWA	x	x	x	x	x	x	x
NKS	N/A	x	x	x	x	x	x
NKM	x	N/A	x	x	x	x	x
NKL	x	x	N/A	x	x	x	x
NSC	x	x	x	N/A	x	x	x
NFE	x	x	x	x	N/A	x	x
NRN	x	x	x	x	x	N/A	x
NSQ	x	x	x	x	x	x	N/A
RSQ	x	x	x	x	x	x	x

Table 2: Comparison of performance between the baseline models and SQUWA, evaluated using AUROC, F1 score, and AUCPR as metrics.

		Testset A			**Testset B**			**Testset C**		
Model	Data	AUROC	F1	AUCPR	AUROC	F1	AUCPR	AUROC	F1	AUCPR
ResNet-34	PPG	0.54 ± 0.01	0.4 ± 0.01	0.25 ± 0.01	0.63 ± 0.01	0.6 ± 0.02	0.53 ± 0.02	0.68 ± 0.01	0.28 ± 0.02	0.23 ± 0.02
LSTM	PPG	0.48 ± 0.01	0.23 ± 0.03	0.21 ± 0.02	0.41 ± 0.02	0.47 ± 0.03	0.39 ± 0.02	0.57 ± 0.02	0.18 ± 0.03	0.12 ± 0.03
ResNet-34 +LSTM	PPG	0.64 ± 0.01	0.43 ± 0.01	0.34 ± 0.02	0.82 ± 0.01	0.71 ± 0.01	0.74 ± 0.01	0.93 ± 0.01	0.56 ± 0.01	0.68 ± 0.01
CMC	PPG	0.76	0.53	0.6	0.88	0.75	0.84	0.94	0.7	0.73
SiamAF	PPG+ECG	**0.87**	0.61	**0.72**	0.9	0.78	0.86	0.94	0.73	0.72
SQUWA	PPG	0.8 ± 0.01	0.56 ± 0.01	0.63 ± 0.01	0.9 ± 0.01	0.8 ± 0.01	0.85 ± 0.02	0.94 ± 0.01	0.73 ± 0. 01	0.75 ± 0.01
SQUWA + CMC	PPG	0.82	0.59	0.66	0.91	0.8	0.85	0.95	0.75	0.79
SQUWA + SCE	PPG	0.84	0.62	0.7	0.89	0.79	0.8	0.94	0.75	0.79
SQUWA + JOL	PPG	**0.87**	**0.63**	0.7	**0.93**	**0.81**	**0.89**	0.94	0.74	0.77
SQUWA + GCE	PPG	**0.87**	0.61	0.71	0.92	0.8	0.88	**0.95**	**0.76**	**0.8**

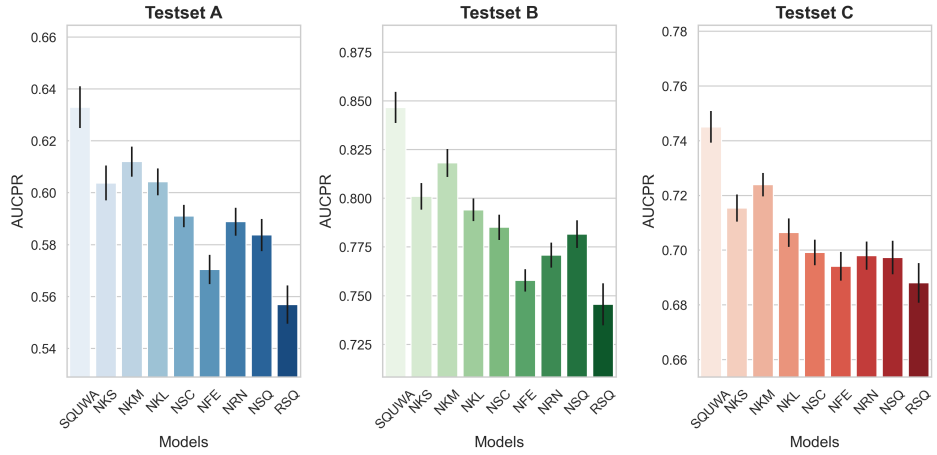

Figure 3: Visualization of an ablation study showing the area under the precision-recall curve (AUCPR) across three test sets.

Figure 4 presents the AUCPR scores in relation to the bad signal quality percentage for the SQUWA model and its variant NSQ that omits SQI integration. The y-axis measures the AUCPR, while the x-axis represents the percentage of the signal considered to be of bad quality based on SQIs from CAM. Each point on the graphs corresponds to AUCPR scores computed from signal samples with a bad quality percentage up to the indicated threshold. For the Testset A, as the threshold for bad signal quality increases, the AUCPR for SQUWA remains relatively stable and even shows a slight improvement, suggesting that the model is robust to varying signal quality. In contrast, the NSQ exhibits a decline in AUCPR,

highlighting the model's dependency on higher signal quality for maintaining performance. In the case of the Testset B, the disparity between the two models becomes more pronounced. The SQUWA maintains its AUCPR scores substantially better as the signal quality worsens compared to the NSQ, which demonstrates a steeper drop. This indicates that the integration of SQI within SQUWA plays a significant role in preserving the model's performance under poor signal conditions. For the Testset C, both models show an increase in AUCPR as the threshold for bad signal quality increases, but SQUWA consistently outperforms NSQ. The SQUWA's AUCPR scores increase more steeply, reinforcing the benefit of SQI integration in managing lower-quality signals. Overall, these figures suggest that SQI integration is an important feature of the SQUWA model, helping to sustain performance across varying levels of signal quality, which is particularly evident when comparing to the NSQ variant that lacks this feature.

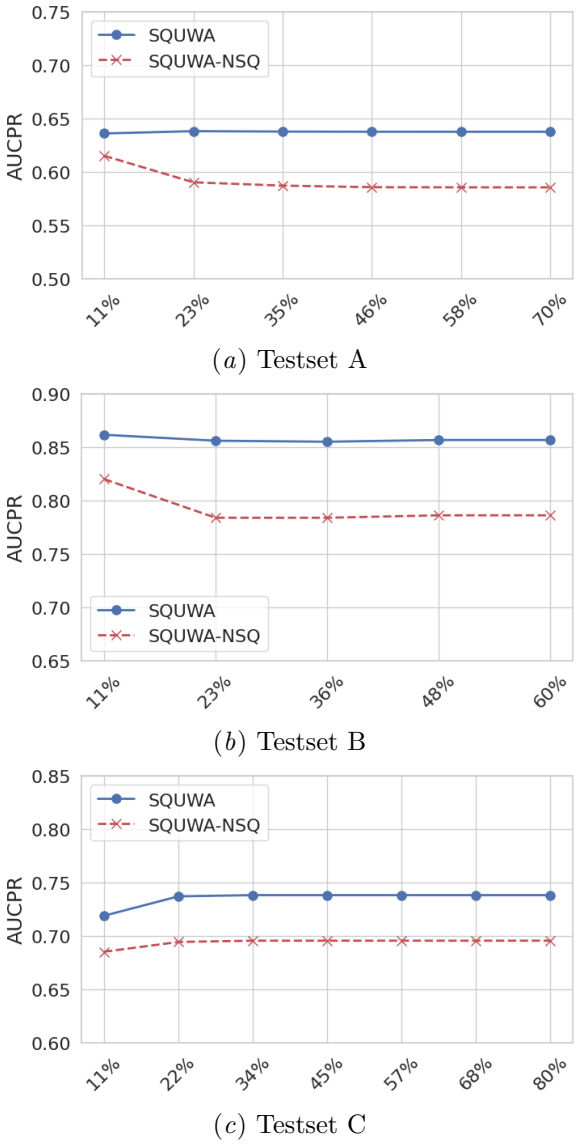

Figure 4: Comparing AUCPR scores of the SQUWA model and its NSQ variant without signal quality integration. The comparison is shown on a graph with AUCPR on the y-axis and the percentage of signal with bad quality on the x-axis.

As shown in Figures 5, we applied the trained SQUWA model on the signal quality dataset mentioned in Section 4.1.2. Figure 5 illustrates an example of a Non-AF signal, with an additional AF example shown in Figure 6. The first subplot depicts the amplitude variations corresponding to the raw PPG over time, while the second subplot visualizes the shape of the combined original signal and its derivatives after being passed through the composite signal generator. The composite signal shows more fine-grained details and contains a rich set of features than the raw PPG signal. In summary, the processed composite signal appears to extract a more comprehensive representation of the physiological characteristics as captured in the raw PPG signal and its temporal derivatives using varying-sized kernels. The purple curve represents the SQIs from SQ model, where a low value means worse signal quality. The red shaded areas represent periods manually annotated as having bad signal quality. It appears that the purple curve, which indicates the assessed signal quality, has valleys that align with the red shaded areas. This suggests that the SQIs are sensitive to the noise in the signal. The heatmap visualizes the attention score matrix and indicate how each time point in the SQIs (horizontal axis) influences each time point in the hidden states derived from the LSTM (vertical axis). Color intensity indicates the strength of the attention. A warmer color indicates higher attention weights, meaning that the SQI at that time point has a large influence on the hidden state from the LSTM at a given time. Each column on the horizontal axis corresponds to a moment in time for the SQI, and each row on the vertical axis corresponds to a moment in time for the hidden states derived from the LSTM. And all the elements of SQI and hidden states

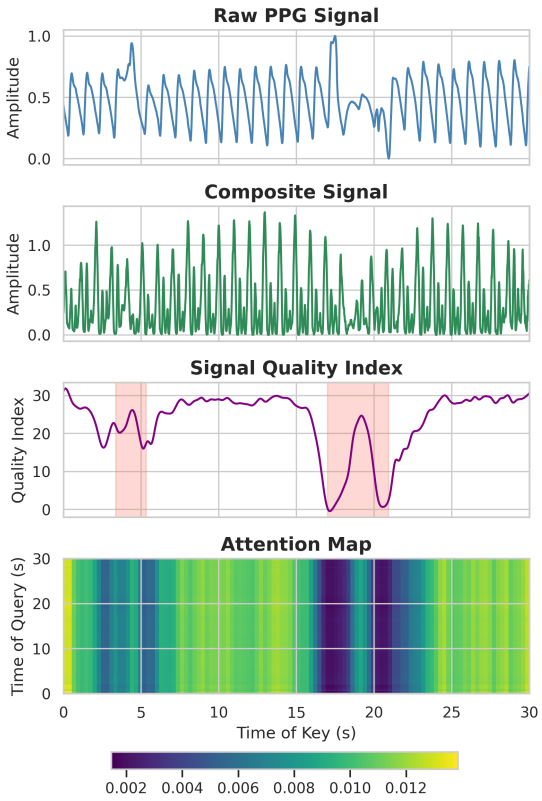

Figure 5: This figure shows a Non-AF PPG signal with poor signal quality segments. The red area highlighted in the third figure indicates the portion of poor quality annotated by a person. The first and the second figures show the raw PPG signal and the signal after the composite signal generator in Figure 3.1. The purple line of the third figure visualizes the signal quality, where a low value indicates poor signal quality

. Additionally, an attention heatmap shows the influence of each SQI component (x-aixs) on the LSTM's hidden states (y-axis), highlighting the impact of sequence segment quality on the LSTM representation.

provide a sequential representation of the 30s input PPG signals. From the heatmap, we can observe that the bright yellow lines or spots indicate time points where the SQIs strongly influences the LSTM's hidden states. Conversely, the darker regions indicate time points that have less influence on the LSTM's hidden states, and these dark regions correspond with the red shaded areas in the SQIs, it suggests that the network is learning to disregard low-quality data.

6. Discussion & Conclusion

Detecting AF using PPG signals is crucial for use cases such as population-wide AF screening using wearable devices. However, a key challenge to realize such a potential of PPG is to account for impact of low signal quality on AF-detection sensitivity, which is important for screening AF at scale, and precision, which is critical to minimize untoward consequences of false detection. In response to this challenge, we present the SQUWA neural network, which employs an attention mechanism designed to prioritize decision-making based on high-quality signal segments while mitigating the negative effects of corrupted segments, thereby enhancing the reliability of AF detection in PPG signals. Using SQUWA, there is no need to rely on using an arbitrary signal threshold to discard PPG siganls of poor quality. When assessing our method using three independent datasets not included in the training data collection, SQUWA outperformed traditional PPG models in classifying AF and Non-AF conditions. An ablation study revealed that the signal quality attention mechanism significantly boosts performance, with each component of the SQUWA model contributing positively to achieving performance seen in the full version of SQUWA. The attention maps validated our theory that the decision-making process favors segments with higher signal quality over those with lower quality. This attribute aligns with the insights of human domain experts, who can identify and tolerate noisy segments in the signals to a certain extent, while still making accurate judgments about AF by focusing on the segments of good quality. The issue of handling noisy time-series data is not unique to AF detection. Therefore, the principles underlying the SQUWA architecture could potentially be adapted for a range of other applications, such as human activity recognition and speech recognition, where similar data quality challenges exist.

It's important to note that alghtough the SQUWA model benefits from integrating the SQIs in the training process, it is not an entirely end-to-end system. The signal quality assessment component does require pre-training on a dataset with annotated signal quality, though the size of this dataset does not need to be substantial. Although we presented three test sets to demonstrate the robustness of SQUWA, more

evaluations are needed to confirm its generalizability. Another limitation is that SQUWA is susceptible to inducing false negatives when artifacts obscure portions of signals where evidence AF is located. In practice, outputs from SQUWA processing consecutive 30-second strips can be further analyzed to enhance the model robustness for AF detection.

Institutional Review Board (IRB) The model development data was sourced from routine bedside monitor usage in the intensive care units at UCSF Medical Center (Institution A), under an IRB-approved waiver for written patient consents (IRB number: 14-13262). Testset B was collected from patients at Emory University Hospital undergoing AF ablation, who consented to wear a study device for PPG signal collection under IRB (00084629). Testset C was collected from routine bedside monitor usage in the acute care units at UCLA Medical Center with an IRB-approved waiver for written consents (IRB 10-000545).

Acknowledgments

This research is supported by the National Institutes of Health (NIH) grant R01HL166233. It is incorporated into the DELTA project (Detecting and Predicting Atrial Fibrillation in Post-Stroke Patients), which has been registered on clinicaltrials.gov.

References

Amir Hosein Afandizadeh Zargari, Seyed Amir Hossein Aqajari, Hadi Khodabandeh, Amir Rahmani, and Fadi Kurdahi. An accurate non-accelerometer-based ppg motion artifact removal technique using cyclegan. *ACM Transactions on Computing for Healthcare*, 4(1):1–14, 2023.

Laith Alzubaidi, Jinglan Zhang, Amjad J Humaidi, Ayad Al-Dujaili, Ye Duan, Omran Al-Shamma, José Santamaría, Mohammed A Fadhel, Muthana Al-Amidie, and Laith Farhan. Review of deep learning: concepts, cnn architectures, challenges, applications, future directions. *Journal of big Data*, 8:1–74, 2021.

Yoshua Bengio, Li Yao, Guillaume Alain, and Pascal Vincent. Generalized denoising auto-encoders as generative models. *Advances in neural information processing systems*, 26, 2013.

Eoin Brophy, Zhengwei Wang, Qi She, and Tomás Ward. Generative adversarial networks in time series: A systematic literature review. *ACM Computing Surveys*, 55(10):1–31, 2023.

Peter H Charlton, John Allen, Raquel Bailón, Stephanie Baker, Joachim A Behar, Fei Chen, Gari D Clifford, David A Clifton, Harry J Davies, Cheng Ding, et al. The 2023 wearable photoplethysmography roadmap. *Physiological measurement*, 44(11):111001, 2023.

Shubhojeet Chatterjee, Rini Smita Thakur, Ram Narayan Yadav, Lalita Gupta, and Deepak Kumar Raghuvanshi. Review of noise removal techniques in ecg signals. *IET Signal Processing*, 14(9):569–590, 2020.

Zailiang Chen, Ziyang Zeng, Hailan Shen, Xianxian Zheng, Peishan Dai, and Pingbo Ouyang. Dn-gan: Denoising generative adversarial networks for speckle noise reduction in optical coherence tomography images. *Biomedical Signal Processing and Control*, 55:101632, 2020.

Peng Cheng, Zhencheng Chen, Quanzhong Li, Qiong Gong, Jianming Zhu, and Yongbo Liang. Atrial fibrillation identification with ppg signals using a combination of time-frequency analysis and deep learning. *IEEE Access*, 8:172692–172706, 2020.

Sumeet S Chugh, Rasmus Havmoeller, Kumar Narayanan, David Singh, Michiel Rienstra, Emelia J Benjamin, Richard F Gillum, Young-Hoon Kim, John H McAnulty Jr, Zhi-Jie Zheng, et al. Worldwide epidemiology of atrial fibrillation: a global burden of disease 2010 study. *Circulation*, 129(8):837–847, 2014.

Oscar Day and Taghi M Khoshgoftaar. A survey on heterogeneous transfer learning. *Journal of Big Data*, 4:1–42, 2017.

Cheng Ding, Ran Xiao, Duc H Do, David Scott Lee, Randall J Lee, Shadi Kalantarian, and Xiao Hu. Log-spectral matching gan: Ppg-based atrial fibrillation detection can be enhanced by gan-based data augmentation with integration of spectral loss. *IEEE Journal of Biomedical and Health Informatics*, 27(3):1331–1341, 2023.

Cheng Ding, Zhicheng Guo, Cynthia Rudin, Ran Xiao, Amit Shah, Duc H. Do, Randall J Lee, Gari Clifford, Fadi B Nahab, and Xiao Hu. Learning

from alarms: A robust learning approach for accurate photoplethysmography-based atrial fibrillation detection using eight million samples labeled with imprecise arrhythmia alarms. *IEEE Journal of Biomedical and Health Informatics*, pages 1–12, 2024. doi: 10.1109/JBHI.2024.3360952.

Haoyuan Gao, Xiaopei Wu, Jidong Geng, and Yang Lv. Remote heart rate estimation by signal quality attention network. In *Proceedings of the IEEE/CVF conference on computer vision and pattern recognition*, pages 2122–2129, 2022.

Meng-Hao Guo, Tian-Xing Xu, Jiang-Jiang Liu, Zheng-Ning Liu, Peng-Tao Jiang, Tai-Jiang Mu, Song-Hai Zhang, Ralph R Martin, Ming-Ming Cheng, and Shi-Min Hu. Attention mechanisms in computer vision: A survey. *Computational visual media*, 8(3):331–368, 2022.

Zhicheng Guo, Cheng Ding, Duc H Do, Amit Shah, Randall J Lee, Xiao Hu, and Cynthia Rudin. Siamaf: Learning shared information from ecg and ppg signals for robust atrial fibrillation detection. *arXiv preprint arXiv:2310.09203*, 2023.

Robert G Hart, Lesly A Pearce, and Maria I Aguilar. Meta-analysis: antithrombotic therapy to prevent stroke in patients who have nonvalvular atrial fibrillation. *Annals of internal medicine*, 146(12):857–867, 2007.

Kaiming He, Xiangyu Zhang, Shaoqing Ren, and Jian Sun. Deep residual learning for image recognition. In *Proceedings of the IEEE conference on computer vision and pattern recognition*, pages 770–778, 2016.

André Henriksen, Martin Haugen Mikalsen, Ashenafi Zebene Woldaregay, Miroslav Muzny, Gunnar Hartvigsen, Laila Arnesdatter Hopstock, and Sameline Grimsgaard. Using fitness trackers and smartwatches to measure physical activity in research: analysis of consumer wrist-worn wearables. *Journal of medical Internet research*, 20(3):e110, 2018.

Daniel Im Im, Sungjin Ahn, Roland Memisevic, and Yoshua Bengio. Denoising criterion for variational auto-encoding framework. In *Proceedings of the AAAI conference on artificial intelligence*, volume 31, 2017.

Yoonsik Kim, Jae Woong Soh, Gu Yong Park, and Nam Ik Cho. Transfer learning from synthetic to real-noise denoising with adaptive instance normalization. In *Proceedings of the IEEE/CVF conference on computer vision and pattern recognition*, pages 3482–3492, 2020.

Ping-Huan Kuo, Ssu-Ting Lin, and Jun Hu. Dnaegan: Noise-free acoustic signal generator by integrating autoencoder and generative adversarial network. *International Journal of Distributed Sensor Networks*, 16(5):1550147720923529, 2020.

Sidrah Liaqat, Kia Dashtipour, Adnan Zahid, Khaled Assaleh, Kamran Arshad, and Naeem Ramzan. Detection of atrial fibrillation using a machine learning approach. *Information*, 11(12):549, 2020.

Carmine Marini, Federica De Santis, Simona Sacco, Tommasina Russo, Luigi Olivieri, Rocco Totaro, and Antonio Carolei. Contribution of atrial fibrillation to incidence and outcome of ischemic stroke: results from a population-based study. *Stroke*, 36 (6):1115–1119, 2005.

Sajad Mousavi, Fatemeh Afghah, and U Rajendra Acharya. Han-ecg: An interpretable atrial fibrillation detection model using hierarchical attention networks. *Computers in biology and medicine*, 127: 104057, 2020.

Deepankar Nankani and Rashmi Dutta Baruah. Atrial fibrillation classification and prediction explanation using transformer neural network. In *2022 International Joint Conference on Neural Networks (IJCNN)*, pages 01–08. IEEE, 2022.

Zhaoyang Niu, Guoqiang Zhong, and Hui Yu. A review on the attention mechanism of deep learning. *Neurocomputing*, 452:48–62, 2021.

Sinno Jialin Pan and Qiang Yang. A survey on transfer learning. *IEEE Transactions on knowledge and data engineering*, 22(10):1345–1359, 2009.

Tania Pereira, Cheng Ding, Kais Gadhoumi, Nate Tran, Rene A Colorado, Karl Meisel, and Xiao Hu. Deep learning approaches for plethysmography signal quality assessment in the presence of atrial fibrillation. *Physiological measurement*, 40 (12):125002, 2019a.

Tania Pereira, Kais Gadhoumi, Mitchell Ma, Xiuyun Liu, Ran Xiao, Rene A Colorado, Kevin J

Keenan, Karl Meisel, and Xiao Hu. A supervised approach to robust photoplethysmography quality assessment. *IEEE journal of biomedical and health informatics*, 24(3):649–657, 2019b.

Monalisa Singha Roy, Rajarshi Gupta, and Kaushik Das Sharma. Photoplethysmogram signal quality evaluation by unsupervised learning approach. In *2020 IEEE Applied Signal Processing Conference (ASPCON)*, pages 6–10. IEEE, 2020.

Dongyeol Seok, Sanghyun Lee, Minjae Kim, Jaeouk Cho, and Chul Kim. Motion artifact removal techniques for wearable eeg and ppg sensor systems. *Frontiers in Electronics*, 2:685513, 2021.

Supreeth Prajwal Shashikumar, Amit J Shah, Qiao Li, Gari D Clifford, and Shamim Nemati. A deep learning approach to monitoring and detecting atrial fibrillation using wearable technology. In *2017 IEEE EMBS international conference on biomedical & health informatics (BHI)*, pages 141–144. IEEE, 2017.

Qingxiong Tan, Mang Ye, Baoyao Yang, Siqi Liu, Andy Jinhua Ma, Terry Cheuk-Fung Yip, Grace Lai-Hung Wong, and PongChi Yuen. Data-gru: Dual-attention time-aware gated recurrent unit for irregular multivariate time series. In *Proceedings of the AAAI Conference on Artificial Intelligence*, volume 34, pages 930–937, 2020.

Daiki Tanaka, Daiki Ikami, Toshihiko Yamasaki, and Kiyoharu Aizawa. Joint optimization framework for learning with noisy labels. In *Proceedings of the IEEE conference on computer vision and pattern recognition*, pages 5552–5560, 2018.

Jessica Torres-Soto and Euan A Ashley. Multi-task deep learning for cardiac rhythm detection in wearable devices. *NPJ digital medicine*, 3(1):116, 2020.

Yisen Wang, Xingjun Ma, Zaiyi Chen, Yuan Luo, Jinfeng Yi, and James Bailey. Symmetric cross entropy for robust learning with noisy labels. In *Proceedings of the IEEE/CVF international conference on computer vision*, pages 322–330, 2019.

Runze Yan, Xinwen Liu, Janine Dutcher, Michael Tumminia, Daniella Villalba, Sheldon Cohen, David Creswell, Kasey Creswell, Jennifer Mankoff, Anind Dey, et al. A computational framework for modeling biobehavioral rhythms from mobile and wearable data streams. *ACM Transactions on Intelligent Systems and Technology (TIST)*, 13(3):1–27, 2022.

Yong Yu, Xiaosheng Si, Changhua Hu, and Jianxun Zhang. A review of recurrent neural networks: Lstm cells and network architectures. *Neural computation*, 31(7):1235–1270, 2019.

Ce Zhang, Young-Keun Kim, and Azim Eskandarian. Eeg-inception: an accurate and robust end-to-end neural network for eeg-based motor imagery classification. *Journal of Neural Engineering*, 18(4): 046014, 2021a.

Oliver Zhang, Cheng Ding, Tania Pereira, Ran Xiao, Kais Gadhoumi, Karl Meisel, Randall J Lee, Yiran Chen, and Xiao Hu. Explainability metrics of deep convolutional networks for photoplethysmography quality assessment. *IEEE Access*, 9:29736–29745, 2021b.

Shucong Zhang, Cong-Thanh Do, Rama Doddipatla, and Steve Renals. Learning noise invariant features through transfer learning for robust end-to-end speech recognition. In *ICASSP 2020-2020 IEEE International Conference on Acoustics, Speech and Signal Processing (ICASSP)*, pages 7024–7028. IEEE, 2020.

Zhilu Zhang and Mert Sabuncu. Generalized cross entropy loss for training deep neural networks with noisy labels. *Advances in neural information processing systems*, 31, 2018.

Bolei Zhou, Aditya Khosla, Agata Lapedriza, Aude Oliva, and Antonio Torralba. Learning deep features for discriminative localization. In *Proceedings of the IEEE conference on computer vision and pattern recognition*, pages 2921–2929, 2016.

Li Zhu, Viswam Nathan, Jilong Kuang, Jacob Kim, Robert Avram, Jeffrey Olgin, and Jun Gao. Atrial fibrillation detection and atrial fibrillation burden estimation via wearables. *IEEE Journal of Biomedical and Health Informatics*, 26(5):2063–2074, 2021.

Yizhe Zhu, Mohamed Elhoseiny, Bingchen Liu, Xi Peng, and Ahmed Elgammal. A generative adversarial approach for zero-shot learning from noisy texts. In *Proceedings of the IEEE conference on computer vision and pattern recognition*, pages 1004–1013, 2018.

Appendix A. Implementation Details

All experiments were conducted on a high-performance computing (HPC) cluster equipped with NVIDIA A100 and V100 GPUs. SQUWA was trained with these hyperparameters: batch size of 1024, and an Adam optimizer with a learning rate of 1e-4, using exponential decay. To prevent overfitting, we employed early stopping, stopping training if the validation loss did not improve for 10 epochs. For the composite signal generator, we used odd kernel sizes: 119 (about 1.5 seconds), 479 (about 6 seconds), and 799 (about 10 seconds), with a sampling frequency of 80Hz. Our architecture includes ResNet 34 for signal quality assessment and ResNet 18 for feature extraction, along with an LSTM with a hidden size of 64.

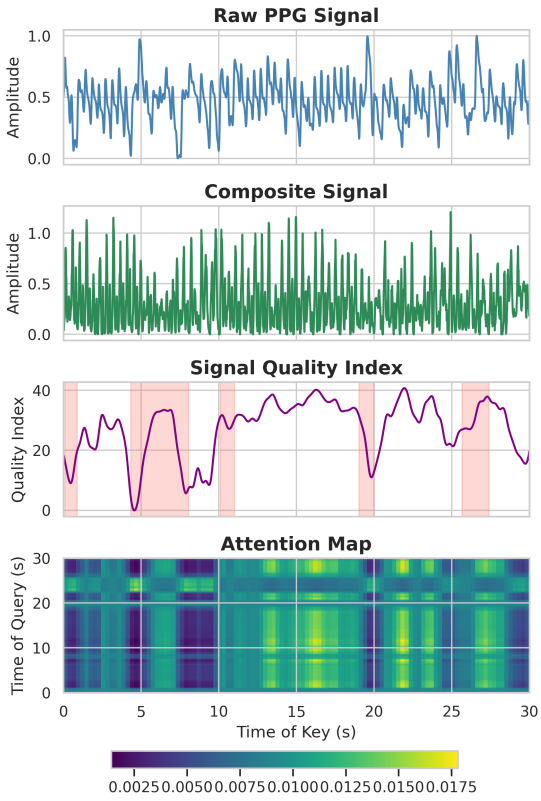

Figure 6: This figure shows an AF PPG signal with segments of low quality.

Appendix B. Attention Map of a AF Sample

Figure 5 shows a Non-AF sample, and we introduce an additional AF example in this section. The AF sample, as shown in Figure 6, exhibits greater and more complex fluctuations compared to the Non-AF sample. But the generated signal quality index successfully identifies the corrupted segments, aligning with the human annotations marked by red shapes in the figure. The attention map reveals that the good quality sections receive higher weights compared to those that are corrupted. This demonstrates that our proposed method still works well for AF signals.

Appendix C. Visualization of Test Samples

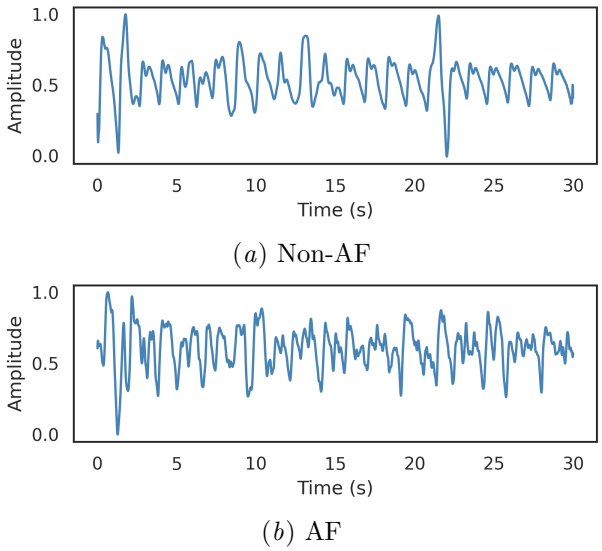

(*a*) Non-AF

(*b*) AF

Figure 7: Accurately classified AF and Non-AF samples from Testset A

In this section, we provide additional instances of accurately classified AF and Non-AF samples for the three datasets: Testset A, as presented in Figure 7, Testset B, as presented in Figure 8, and Testset C, as presented in Figure 9. These EGM signals contain corrupted parts, demonstrating that SQUWA is able to accurately identify AF despite imperfections in the EGM signals.

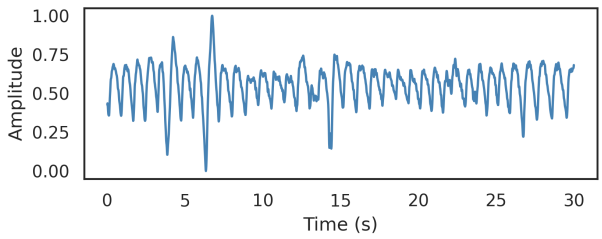

(*a*) Non-AF

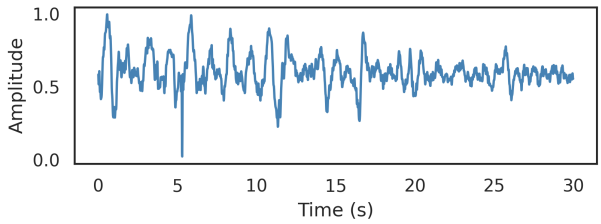

(*b*) AF

Figure 8: Accurately classified AF and Non-AF samples from Testset B

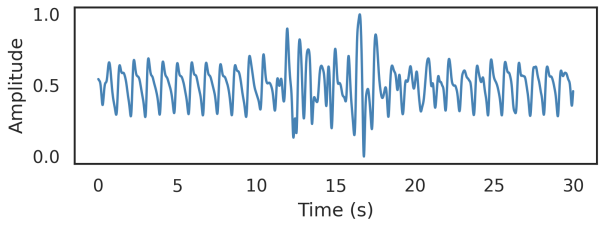

(*a*) Non-AF

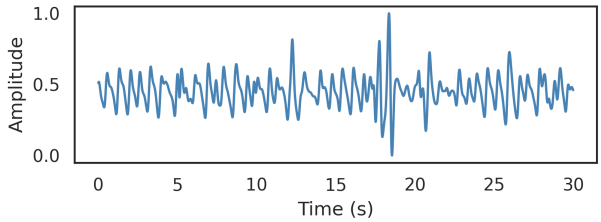

(*b*) AF

Figure 9: Accurately classified AF and Non-AF samples from Testset C